Article

Chitosan-Based Grafted Cationic Magnetic Material to Remove Emulsified Oil from Wastewater: Performance and Mechanism

Sicong Du, Chuang Liu, Peng Cheng and Wenyan Liang *

Beijing Key Lab for Source Control Technology of Water Pollution, College of Environmental Science and Engineering, Beijing Forestry University, Beijing 100083, China; dsc1008@126.com (S.D.); lcliuchuang@hotmail.com (C.L.); chengpeng3910@163.com (P.C.)
* Correspondence: lwy@bjfu.edu.cn

Abstract: In order to remove high-concentration emulsified oil from wastewater, a chitosan-based magnetic flocculant, denoted as FS@CTS-P(AM-DMC), was employed in this present study. The effects of factors including the magnetic flocculant dose, pH values, and coexisting ions were investigated. A comparative dosing mode with the assistance of polyacrylamide (PAM) was also included. The evolution of floc size was studied using microscopic observation to investigate the properties of flocs under different pH values and dosing modes. Particle image velocimetry (PIV) and extended Deryaguin–Landau–Verwey–Overbeek models were utilized to illustrate the distribution and velocity magnitude of the particle flow fields and to delve into the mechanism of magnetic flocculation. The results showed that FS@CTS-P(AM-DMC) achieved values of 96.4 and 74.5% for both turbidity and COD removal for 3000 mg/L of simulated emulsified oil. In the presence of PAM, the turbidity and COD removal reached 95.7 and 71.6%. In addition, FS@CTS-P(AM-DMC) demonstrated remarkable recycling and reusability performances, maintaining effective removal after eight cycles. The strength and recovery factors of magnetic flocs without PAM reached 69.3 and 76.8%, respectively. However, with the addition of PAM, they decreased to 46.73 and 51.47%, respectively. During the magnetophoretic processes, FS@CTS-P(AM-DMC) and oil droplets continuously collided and aggregated, forming three-dimensional network aggregates. Moreover, the magnetic floc generated a swirling motion, and the residual emulsified oil droplets could be further captured. Emulsified oil droplets were primarily removed through charge neutralization under acidic conditions. Under neutral and alkaline conditions, magnetic interactions played a major role in magnetic flocculation.

Keywords: emulsified oil; magnetic flocculation; Fe_3O_4; chitosan; methacryloyloxyethyl trimethyl ammonium chloride; particle image velocimetry; Deryaguin–Landau–Verwey–Overbeek model

1. Introduction

Due to the rapid development of the oil industry, including sectors such as crude oil extraction, metallurgical machinery, and other petrochemical industries, the generation of emulsified, oily wastewater has become increasingly prevalent [1,2]. Simultaneously, there is also a large amount of emulsified oil in the wastewater generated by this industry [3]. The abundance of emulsifiers or surfactants present in the wastewater contributes to spatial resistance and electrostatic repulsion among the oil droplets. These emulsified oil droplets become more stable and difficult to settle down [4]. If emulsified, oily wastewater is released into the environment without effective treatment, it will cause serious harm to the ecosystem and human health [5]. On the other hand, emulsified oil not only corrodes metal equipment easily but also increases the risk of pollution in subsequent petroleum processing [6]. Therefore, it is necessary to remove the oil droplets in emulsified wastewater before discharge.

Numerous techniques are available for the removal of emulsified oil droplets, encompassing air flotation [7], membrane separation [8,9], adsorption [10], flocculation [11–13],

and biological treatment [14]. Magnetic flocculation (MF) is a technique that integrates conventional flocculation with magnetic separation, frequently applied in water treatment to remove or separate heavy metals, ultrafine particles, and minerals [15–17]. The naked Fe_3O_4 is frequently used due to its simple preparation and structure. However, the negative charges of both the naked Fe_3O_4 and emulsified oil droplets lead to a remarkably low flocculation efficiency [18]. Therefore, conventional flocculants, such as polymeric aluminum chloride and polyacrylamide (PAM), are often dosed as assistants for the naked Fe_3O_4 [19–21]. While this approach enhances the removal efficiency of emulsified oil, it complicates the operation and leaves a certain number of flocculants in the water, potentially posing environmental risks.

The naked Fe_3O_4 can be modified by coating specific chemicals to alter its surface properties, enabling the modified Fe_3O_4 to exhibit a similar performance to that of traditional flocculant assistants [22]. These materials possessed the excellent flocculant effects on various substances, such as TiO_2 nanoparticles, kaolin, and microalgae [23–25]. When it comes to the removal of emulsified oil droplets, Fe_3O_4 is often modified using propylene oxide-ethylene oxide block polyether [26] and N-(aminoethyl)-aminopropyl functionalized silica [27]. A polyvinylpyrrolidone-coated magnetic flocculant can also be used for treatment of emulsified, oily wastewater [28]. However, these modified materials primarily act as magnetic demulsifiers, resulting in a reduced efficiency in oil collection. To address this issue, cationic polymers were introduced to the surface of Fe_3O_4 to capture negatively charged emulsified oil droplets. Examples include chitosan [29], dimethyl diallyl ammonium chloride [30], and poly(dimethyl-diallyl-ammonium chloride) [31]. Through self-assembly, a self-crosslinked admicelle was grafted onto the surface of Fe_3O_4, and it maintained a good treatment effect after four cycles [32]. These materials exhibit a commendable efficiency in treating emulsified, oily wastewater, particularly at low concentrations ranging from 10–200 mg/L. Nevertheless, it is noteworthy that in some industrial settings, the concentration of emulsified, oily wastewater can soar as high as 3000 mg/L [33]. Therefore, it is necessary to utilize magnetic materials for the effective treatment of highly concentrated, emulsified, oily wastewater.

Drawing from our previous study, a cationic magnetic flocculant, named FS@CTS-P(AM-DMC), achieved a remarkable separation effectiveness in high-turbidity kaolin wastewater. Here, $Fe_3O_4@SiO_2$ (abbreviated as FS) served as the magnetic core, while chitosan (CTS), acrylamide (AM), and methacryloyloxyethyl trimethyl ammonium chloride (DMC) acted as the cationic functional layer [34]. This cationic layer boasted a high relative molecular weight, positive charge density, and long graft chain, all of which contributed to its effectiveness. Given these attributes, FS@CTS-P(AM-DMC) is being considered as a candidate for capturing emulsified oil droplets present in high concentrations.

The magnetic flocculation process is typically facilitated by the various interaction forces that exist between the flocculant and pollutant, including van der Waals forces, electrostatic forces, and magnetic forces [35]. Due to the distinct surface charges, sizes, densities of oil droplets, and solution pH values, the interaction between the magnetic flocculant and emulsified oil droplet is a highly intricate process. Previous studies have delved into this interaction through adsorption kinetic modeling, primarily attributing it to electrostatic interactions between the charges on the material surface and the emulsified oil droplets [36,37]. However, this approach overlooked interaction forces and their potential influences.

The Deryaguin–Landau–Verwey–Overbeek (DLVO) theory and its extended model have been widely used in investigating the aggregation and dispersion processes of magnetic materials with kaolin, minerals, and ultrafine particles [24,38–41]. These theories have revealed that, apart from the van der Waals force and electrostatic force, the Lewis acid–base force and magnetic force also influence the aggregation and dispersion behaviors between flocculants and solid particles. Nonetheless, emulsified oil droplets differ significantly from solid particles. They typically consist of both oil and surfactants, exhibiting a far more complex chemical composition and surface properties. There is a pressing need to

conduct a thorough investigation using DLVO and EDLVO theories. Thus, the interaction force between the material and the emulsified oil droplets is analyzed in a more detailed way, which in turn enriches the mechanism of magnetic flocculation for the treatment of emulsified, oily wastewater.

Moreover, there are limited reports on the magnetophoretic flow field and floc movement behaviors during magnetic separation processes. Particle image velocimetry (PIV) is a well-established and versatile non-contact optical technique that has garnered widespread usage in various fields related to fluid dynamics [42]. It holds a pivotal position in research conducted in the fields of aeronautical, mechanical, and civil engineering [43–45]. The PIV technique enables the measurement of particle displacement across specific time intervals, thereby revealing the instantaneous velocity distribution within fluid flow fields. Consequently, it offers a quantitative description of the actual state of the magnetic field [46]. Spatial variations in the motion and velocity of oil-containing flocs during magnetic separation can be elucidated using PIV.

In this study, FS@CTS-P(AM-DMC) was employed to treat emulsified, oily wastewater, and a thorough evaluation of its flocculation performance was assessed under diverse conditions. A systematic investigation was conducted into the reutilization of FS@CTS-P (AM-DMC). A comparative analysis was conducted with the PAM-assisted strategy. The sizes of magnetic flocs in fragmentation and regeneration processes were monitored online. The analysis also included examining the morphological changes and fractal dimensions of the magnetic flocs. The extended DLVO theories and PIV techniques were invoked to study the interaction between the FS@CTS-P(AM-DMC) and emulsified oil droplets.

2. Materials and Methods

2.1. Chemicals and Materials

$FeCl_3 \cdot 6H_2O$, $FeCl_2 \cdot 4H_2O$, $(NH_4)_2S_2O_8$, and PAM (molecular weight $\geq$ 3,000,000) were purchased from Sinopharm Chemical Reagent (Beijing, China). Chitosan (deacetylation degree of 80–95%), tetraethoxysilane (TEOS, >99% GC), sodium dodecyl sulfonate (SDS), DMC (75 wt.%), and AM were obtained from Sigma-Aldrich (Shanghai, China). Additionally, 0# diesel was purchased from China National Petroleum Corporation. Other reagents including ethanol, HCl, and NaOH were of analytical grade and purchased from a local chemical reagent company.

2.2. Preparation of Emulsified, Oily Wastewater

The emulsified, oily wastewater was prepared by vigorous stirring at room temperature using an experimental agitator (ZR4-6, Resources Water Technology Development, Shenzhen, China). The 0.50 g 0# diesel was added into 495 mL of distilled water and stirred at 1000 rpm for 30 min. Then, the solution was added to 5 mL of 10 g/L SDS solution and stirred for 90 min. The pH values of the emulsion were adjusted using 0.1 mol L-1 HCl and NaOH. The emulsion exhibited the following characteristics: pH value of 7.6 $\pm$ 0.5, oil concentration of 1000 mg L^{-1}, turbidity of 950 $\pm$ 50 NTU, and COD of 1150 $\pm$ 50 mg L^{-1}.

2.3. Synthesis of FS@CTS-P(AM-DMC)

FS@CTS-P(AM-DMC) was synthesized using the free radical copolymerization methods described in our previous work [34]. Briefly, $FeCl_3 \cdot 6H_2O$ and $FeCl_2 \cdot 4H_2O$ were used as the precursors to synthesize Fe_3O_4 nanoparticles. Subsequently, the Fe_3O_4 nanoparticles were coated with silica using the Söber method. $Fe_3O_4@SiO_2$ particles were added into the acetic acid solution containing chitosan. Subsequently, DMC and AM were sequentially added. Finally, ammonium persulfate was introduced as an initiator to initiate polymerization.

2.4. Characterization and Analysis

The functional groups of FS@CTS-P(AM-DMC) were determined using FT-IR spectroscopy (Nicolet 6700, Thermo Fisher Scientific, Waltham, MA, USA). The zeta potential

(ZP) of water samples was measured using a Zetasizer (Malvern Zetasizer Nano ZS90, Malvern, UK). The contact angle of the material and the surface tension components of emulsified oil were measured at an ambient temperature using an optical contact angle meter (OCA 20, Dataphysics, Filderstadt, Germany). The turbidity of the supernatant was measured using a turbidity meter (2100Q, HACH, Loveland, CO, USA). The COD was determined using rapid digestion spectrophotometry (HJ 828-2017, National Environmental Protection Standard, Beijing, China).

2.5. Flocculation Operation

The flocculation experiments were carried out at room temperature with a beaker tester (ZR4-6, Resources Water Technology Development, Shenzhen, China). After FS@CTS-P(AM-DMC) was added to 200 mL of emulsified, oily wastewater, the mixture was vigorously stirred at 400 rpm for 10 min. Then, it was left to stand for 3 min under an applied magnetic field (a NdFeB permanent magnet, $L \times W \times H = 46 \times 46 \times 22$ mm^3, 0.43 T, $\nabla B < 40$ T/m). Measurements of the turbidity, COD, and zeta potential were conducted on the supernatant collected from a depth of 5 cm below the surface.

To investigate the effects of cationic PAM, a PAM solution (1 g/L) and FS@CTS-P(AM-DMC) were simultaneously added to flocculation beakers at different dosages. The effects of the FS@CTS-P(AM-DMC) (300–2000 mg/L), PAM dosages (0–20 mg/L), stirring time (1–15 min), magnetic separation time (1–15 min), pH values (3.0–11.0), coexisting ions (Ca^{2+}, Mg^{2+}, K^+, and Na^+), and magnetic field strength (0.04, 0.13, and 0.43 T) were evaluated. The following basic conditions were established: pH 7.0, stirring at 400 rpm for 10 min, a dose of 2000 mg/L FS@CTS-P(AM-DMC), and a magnetic separation of 3 min. For the dose of 1000 mg/L FS@CTS-P(AM-DMC) combined with 2 mg/L PAM, the conditions for the flocculation experiment were identical to those mentioned above.

2.6. Distribution of Floc Size

Online measurements of the magnetic floc size were conducted using the Mastersizer 3000 (Malvern 3000, Malvern, UK). The process began with magnetic flocculation at 400 rpm for 10 min, and magnetic separation for 3 min. Then, the magnetic flocs were broken at a stirring speed of 400 rpm for 1 min. Subsequently, the magnet was repositioned beside the beaker for an additional 3 min to regenerate the flocs. During this process, the suspension was continuously pumped into the sample pool at 30 mL/min, and the floc particle size was measured every 20 s. The floc size was represented by the median diameter of equal volume (D_{50}). The strength factor, recovery factor, and growth rate of the floc were calculated using Equation (1), Equation (2), and Equation (3), respectively.

$$\text{Strength Factor (\%)} = d_2 / d_1 \times 100\%, \tag{1}$$

$$\text{Recovery Factor (\%)} = (d_3 - d_2)/(d_1 - d_2) \times 100\%, \tag{2}$$

$$\text{Growth rate} = \Delta\text{size}/\Delta\text{time} \tag{3}$$

where the d_1, d_2, and d_3 (μm) are the average floc sizes in the new stable stage before crushing, after crushing, and after regrowth, respectively.

2.7. Recycling Experiment

After flocculation, the magnetic oil flocs were collected, dispersed in 5 mL of absolute ethanol, and ultrasonicated for 1 min to separate the FS@CTS-P(AM-DMC) from the flocs. FS@CTS-P(AM-DMC) was collected using an external magnet, subjected to three alternating washes with deionized water and absolute ethanol, and reused following freeze drying. The infrared spectrum of detached FS@CTS-P(AM-DMC) was measured. The reusability of FS@CTS-P(AM-DMC) was assessed based on the turbidity removal efficiency.

2.8. Microscopic Image Analysis

Under the optimal dose and varying pH levels (5.0, 7.0, and 9.0), the flocs were collected during the rapid stirring stages and placed on slides for observation with an optical microscope (BX 51, Olympus, Tokyo, Japan). Image-Pro Plus v.6.0 (Media Controbernetics) was employed to measure the image area (A) and projected perimeter (L) of the flocs. The fractal dimension (D_f) of the floc was obtained by calculating the slope of the linear regression line from plotting ln(A) against ln(L), as shown by Equation (4).

$$\ln(A) = D_f \times \ln(L) \tag{4}$$

2.9. PIV Measurement of Magnetophoretic Flow Field

A PIV system encompassing a laser illumination device, a high-speed charge-coupled device (CCD) camera, and process control and image processing software was utilized for tracking the movement and flow velocity of flocs throughout the magnetic separation process (Figure S1). This experiment utilized the laser transmitter to emit high-intensity laser beams for tracking the flocs, employing a double-pulse laser configuration. The CCD camera captured two consecutive images of the measurement area within a specific time interval to generate two PIV frames. During image acquisition, it was ensured that the positions of the light source and the CCD camera were perpendicular to each other. Both devices were synchronized with the computer through a synchronizer. After rapidly stirring at 400 rpm for 10 min, the magnet was placed adjacent to the container to initiate magnetic separation. The flow field data and particle motion trajectory images were captured with a time interval of 25 ms, accumulating a total of 19,200 images. These images were analyzed using MicroVec 3.6.5 (Cube Tiandi Ltd., Beijing, China) and TecPlot 360 (TecPlot Inc., Washington, DC, USA) software to obtain flow field velocities and particle motion trajectory information.

2.10. Interaction Energy Analysis

The DLVO, EDLVO, and MDLVO theories were used to analyze the interaction energy (van der Waals, electrostatic, Lewis acid–base, and magnetic interaction forces). The relevant formulas and parameters used for calculating the interaction energy were provided in the Supplementary Information S2.

2.11. Statistical Analysis

A one-way analysis of variance (ANOVA) was performed with SPSS Statistics 20.0 software (SPSS Inc., Chicago, IL, USA). The results are presented as mean values ± standard deviations (SD). Significant differences were considered if $p < 0.05$.

3. Results and Discussion

3.1. Flocculation Performance

3.1.1. Effects of Flocculant Dose

The effects of dosing were evaluated using two dosing modes. One mode involved solely adding FS@CTS-P(AM-DMC), while the other encompassed concurrent dosing with PAM. As shown in Figure 1a, in the absence of PAM, a turbidity removal of 81.3% was achieved with 300 mg/L FS@CTS-P(AM-DMC). When the dose increased to 1000 mg/L, the removal efficiency climbed to 92.5%. However, increasing the dose beyond 1000 mg/L did not result in apparent improvements, as evidenced by a turbidity removal of 96.4% at 2000 mg/L. Additionally, compared to previously reported magnetic flocculants, FS@CTS-P(AM-DMC) demonstrated excellent efficiency in treating emulsified, oily wastewater (Table S6).
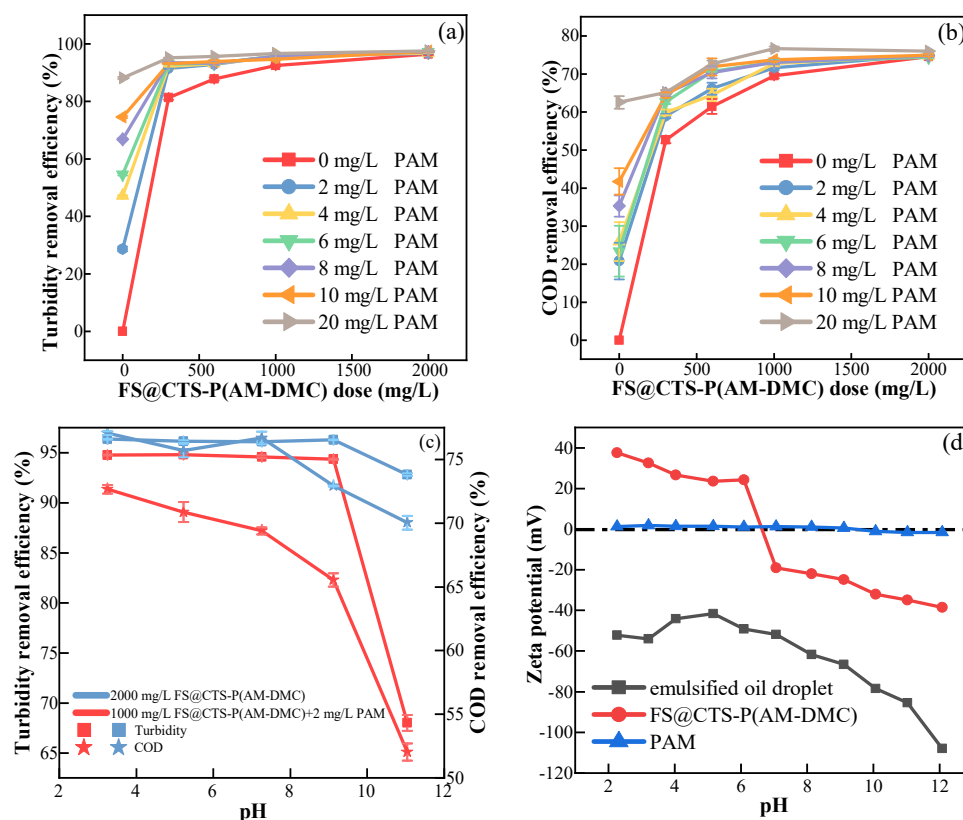
Figure 1. The effect of the (**a**,**b**) dose and (**c**) pH value on the turbidity removal and COD removal using FS@CTS-P(AM-DMC) and PAM. (**d**) Zeta potential of emulsified oil droplet. Stirring speed = 400 r/min. Stirring time = 10 min. Settling time = 3 min.

To investigate the effect of flocculant dose on various initial oil concentrations, experiments were carried out with oil concentrations from 200 to 3000 mg/L. Even when the initial oil concentration increased to 3000 mg/L, the removal of turbidity and COD still reached 98.7 and 88.9%, respectively, under 5000 mg/L FS@CTS-P(AM-DMC) (Figure S2d). This dose is evidently lower compared to the 100 g/L used in other studies for 3000 mg/L oil [47].

As illustrated in Figure 1b, the COD removal trend closely mirrored the turbidity removal. However, the overall removal efficiency was much lower than that of turbidity. Specifically, at a dose of 1000 mg/L FS@CTS-P(AM-DMC), the COD removal only amounted to 69.4%. This was primarily attributed to the presence of dissolved oil compounds and excess surfactants in the water. The removal effect of dissolved organic matter was less effective than that of the oil droplets.

When PAM was dosed alone, it also showed a certain treatment effect (Figure 1a). Although the turbidity removal was only 28.7% at 2 mg/L PAM, it markedly improved to 88.1% at 20 mg/L (Figure 1a), whereas the high dose of 20 mg/L led to residual PAM in the water [48]. Notably, the removal efficiency was greatly increased when FS@CTS-P(AM-DMC) was assisted with PAM. The combination of 300 mg/L FS@CTS-P(AM-DMC) with 2 mg/L PAM achieved a turbidity removal of 91.5%, which was comparable to that achieved with 1000 mg/L FS@CTS-P(AM-DMC). Furthermore, the removal efficiency increased to 95.7% when 1000 mg/L FS@CTS-P(AM-DMC) was used with 2 mg/L PAM. PAM enhanced the removal of emulsified oil droplets primarily through its net catching and sweeping actions [49]. Therefore, the addition of PAM conspicuously reduced the required dose of FS@CTS-P(AM-DMC).

3.1.2. Effects of pH Values

Because the pH value influences the surface properties of flocculants and emulsified oil droplets, it serves as an important factor in the magnetic flocculation process [50,51]. Based on the aforementioned findings, two dosing modes were chosen for the investigation, namely 2000 mg/L FS@CTS-P(AM-DMC) and the combination of 1000 mg/L FS@CTS-P(AM-DMC) with 2 mg/L PAM.

As shown in Figure 1c, the 2000 mg/L FS@CTS-P(AM-DMC) achieved a satisfactory removal performance (96.0–96.3%) within pH 3.0–9.0. From Figure 1d, the emulsified oil droplets exhibited a negative potential at pH 2.0–12.0, while the point of zero charge (pH_{PZC}) of FS@CTS-P(AM-DMC) was determined to be 6.6. Consequently, charge neutralization emerged as the predominant mechanism driving the flocculation process at pH 3.0–6.6. However, both the material and oil droplets were electronegative when pH > 6.6, indicating ineffective charge neutralization. Nevertheless, FS@CTS-P(AM-DMC) still maintained a great removal effect at pH 7.0–9.0. Based on subsequent EDLVO and MDLVO calculations (detailed in Section 3.3.4), electrostatic repulsion was minimal, and there was no energy barrier across a wide interaction distance range (0–200 μm) at pH 7.0 and 9.0. The FS@CTS-P(AM-DMC) could aggregate with emulsified oil droplets through magnetic attraction forces. However, an obvious decrease to 92.8% was observed at pH 11.0. According to the EDLVO and MDLVO calculations, while there was no energy barrier between the magnetic materials, the electrostatic repulsion with the oil droplets was notably higher than that at 9.0. Compared to using the magnetic material alone, the influence of a pH of 11.0 was much more pronounced when PAM was added. The removal efficiency decreased sharply to 68.0% due to the hydrolysis of PAM under alkaline conditions, which weakened its net catching and sweeping actions [52].

The trend in COD removal presented a similar pattern to turbidity removal across different pH values (Figure 1c). However, the influence of pH on COD removal was apparently greater than on turbidity. It can be noted that the decline in turbidity removal commenced at pH 9.0, whereas the decrease in COD removal started from pH 7.0. Additionally, the inclusion of PAM rendered COD removal less effective under alkaline conditions. At pH 11.0, the COD removal efficiency for FS@CTS-P(AM-DMC) alone decreased to 70.03%, whereas the inclusion of PAM caused a sharp decrease to 52.0%. This decrease could be attributed to two primary reasons. Firstly, the electric double layer on the surfaces of the emulsified oil droplets was compressed under alkaline conditions, thereby diminishing the interfacial film of the oil droplets and facilitating the breakdown and dispersal of emulsified oil into the water [53]. Secondly, the hydrolysis of PAM resulted in the contraction of PAM chains, reducing their ability to effectively capture emulsified oil droplets under strongly alkaline conditions [54]. Although PAM reduced the required amount of FS@CTS-P(AM-DMC), the alkaline environment brought about a greater impact on emulsified oil removal.

3.1.3. Effects of Stirring and Settling Time

In traditional flocculation processes, two stirring stages—rapid and slow—are typically employed [22]. However, magnetic flocculation differs, as it can achieve a satisfactory removal efficiency with rapid stirring alone [24]. Therefore, optimizing the rapid stirring time is conducive to dispersing flocculants and promoting the formation of flocs.

As depicted in Figure 2a, there were no significant differences in the turbidity removal between two dosing modes ($p > 0.05$), namely 2000 mg/L FS@CTS-P(AM-DMC) and 1000 mg/L FS@CTS-P(AM-DMC) + 2 mg/L PAM. With the increase in the stirring time from 2 to 10 min, the turbidity removal raised from approximately 90% to 96%. Extending the duration to 15 min did not yield an apparent improvement, as the removal efficiency remained at 95%. However, prolonging the stirring time resulted in an obvious decline in the COD removal. Compared to the 72.3 and 72.7% at 10 min for the two dosing modes, respectively, the removal efficiencies at 15 min sharply dropped to 69.5 and 71.3%. Excessive stirring disrupted the formed magnetic flocs, resulting in the leakage of oily droplets into the water.
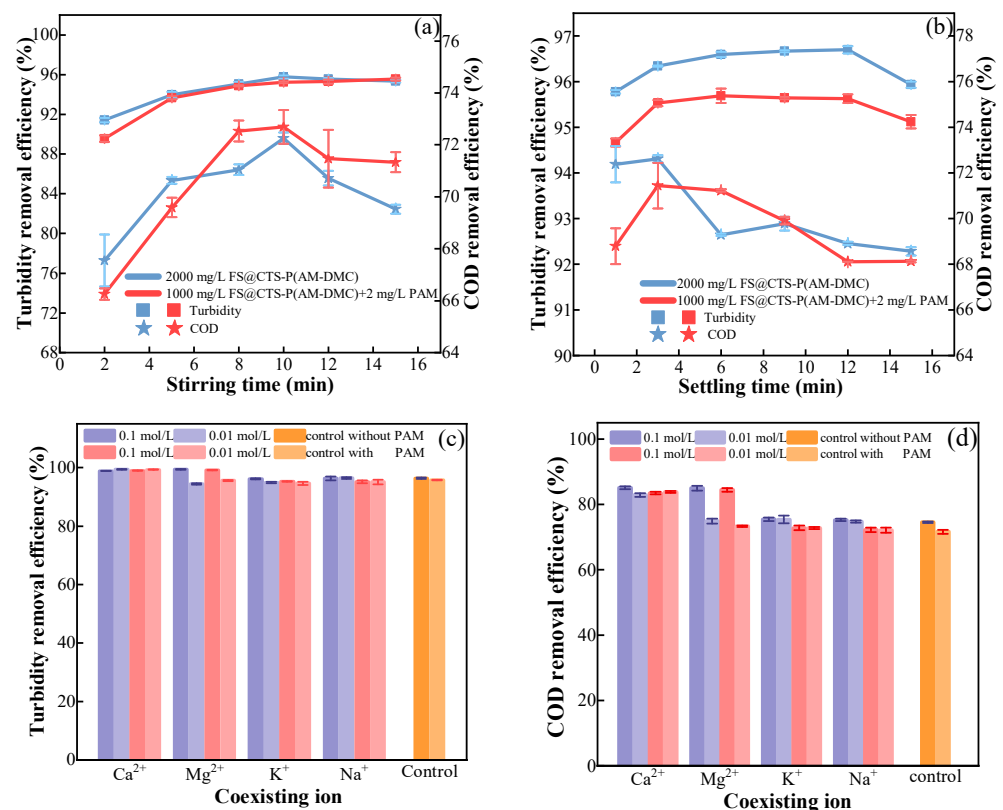
Figure 2. The effects of (**a**) stirring time, (**b**) settling time, and (**c,d**) coexisting ions. Dosing mode: 2000 mg/L FS@CTS-P(AM-DMC) and 1000 mg/L FS@CTS-P(AM-DMC) + 2 mg/L PAM. pH = 7.0. Stirring speed = 400 rpm.

For the settling process, the turbidity removal under the addition of PAM was significantly lower than that only using FS@CTS-P(AM-DMC) ($p < 0.05$). Similarly, an excessive settling time was also detrimental to the removal of COD (Figure 2b). For both dosing modes, the optimal COD removal was realized at 3 min, namely 72.6 and 71.4%, respectively. However, following a settling period of 15 min, both the turbidity and COD removal decreased to 68.6 and 68.1%, respectively. The extended settling time led to a small amount of oil being released into the water. The impact of the settling time differed from the magnetic flocculation of algal cells and aerobic granular sludge [55,56], because solid particles were more difficult to detach from the flocs. The strong buoyancy of oil droplets made them susceptible to floating, particularly with an extended settling time.

3.1.4. Effects of Coexisting Ions

In practical applications, emulsified, oily wastewater typically comprises numerous inorganic ions. In particular, the cationic ions have profound influences on the interfacial tension between water and oil as well as oil–water separation performance [4,24,57]. Therefore, K^+, Na^+, Ca^{2+}, and Mg^{2+} were selected for the investigation in this study. As shown in Figure 2c,d, K^+ and Na^+ exerted no significant effects on either the turbidity or COD removal compared with the controls ($p > 0.05$). Due to the weak Coulomb forces of monovalent ions, the influence of K^+ and Na^+ on the removal processes was negligible [58]. Contrastingly, the divalent ions, such as Ca^{2+} and Mg^{2+}, significantly enhanced the flocculation performance for both dosing modes ($p < 0.05$). The application of 2000 mg/L FS@CTS-P(AM-DMC) achieved an impressive removal of 99.4% for turbidity and 82.9% for COD at 0.01 mol/L Ca^{2+}. Moreover, with the escalation in the concentrations of these ions, there was a corresponding augmentation in the removal efficiency. This was due to the divalent cations possessing a stronger ability to compress the double electric layer and

offering more effective binding sites [59,60], thereby exerting a greater anchoring effect for the flocculant.

3.1.5. Effects of Magnetic Field Strength

The influence of the magnetic field strength on the flocculation efficiency was examined. As presented in Figure S3, the magnetic field strength had significant effects on the removal of emulsified oil droplets ($p < 0.05$). For both dosing modes, the optimal removals for turbidity and COD were 96.8% and 95.7% as well as 74.7% and 72.6% at 0.43 T, respectively (Figure S3a,b). An enhanced magnetic field strength proved beneficial in improving the removal efficiency (Figure S3a,b). The separation of emulsified oil droplets occurred, owing to a combination of forces, including magnetic forces, van der Waals forces, and fluid motion [61]. According to the MDLVO formulation, the degree of magnetic interaction increased with the strength of the saturation magnetization and size of the particles [62]. The high magnetic field strength enhanced the probability of collision and combination among magnetic flocs, leading to the formation of sizable magnetic conglomerates (Yu et al., 2020). During the magnetophoretic process, magnetic fields attract magnetic flocs, which could also be mutually attracted to each other through magnetic force. However, the removal efficiency decreased significantly when using 1000 mg/L FS@CTS-P(AM-DMC) with 2 mg/L PAM at 0.04 T and 0.13 T ($p < 0.05$). This was attributed to the incorporation of PAM, which interfered with the collisions and combinations of the flocs at lower magnetic field strengths, thereby preventing the further removal of emulsified oil droplets. Hence, the exclusive usage of FS@CTS-P(AM-DMC) exhibited a superior removal effect under different magnetic field strengths. Additionally, a higher magnetic field strength facilitated improved the magnetic separation efficiency and resulted in faster magnetic separation speeds.

3.2. Recovery and Reuse

From the economic and practical feasibility standpoint, the recovery and reuse of FS@CTS-P(AM-DMC) play a crucial role in the magnetic flocculation [63]. As demonstrated in Figure 3a, the turbidity removal decreased from 96.9% to 79.0% after eight cycles of reuse at 2000 mg/L FS@CTS-P(AM-DMC). However, under the PAM-assisted conditions, the removal efficiency slightly increased to 82.4%. This enhancement might be attributed to the reconfiguration and addition of PAM in each cycle. The FTIR spectra showed that the peak positions remained unchanged after the recycling and reuse processes, suggesting that the structural integrity of FS@CTS-P(AM-DMC) was preserved (Figure 3c,d). The peaks at 1173 and 1176 cm^{-1} corresponded to the C-O-C in CTS [64]. The vibrational peaks at 1635 and 1629 cm^{-1} were attributed to the -C=O bond in AM [65]. The characteristic absorption peaks of the submethyl and methyl groups of DMC were detected at 1443 and 1450 cm^{-1} as well as 953 and 947 cm^{-1} [66,67]. Notably, there were no new functional groups observed, indicating the stability of the material.

Furthermore, despite washing several times, there was no residual oil attached to the material surface. However, there was an apparent decrease in the intensity of the characteristic peaks. Ultrasonic vibration during the cleaning processes caused the detachment of surface functional groups, which in turn reduced the binding sites on FS@CTS-P(AM-DMC). This decrease resulted in the descend catchment of oil droplets. Nevertheless, the removal efficiency remained at 80% after eight cycles. Additionally, the saturation magnetization slightly decreased from 52.1 and 50.1 emu/g after eight cycles (Figure 3b), suggesting that FS@CTS-P(AM-DMC) still maintained its strong magnetic response.
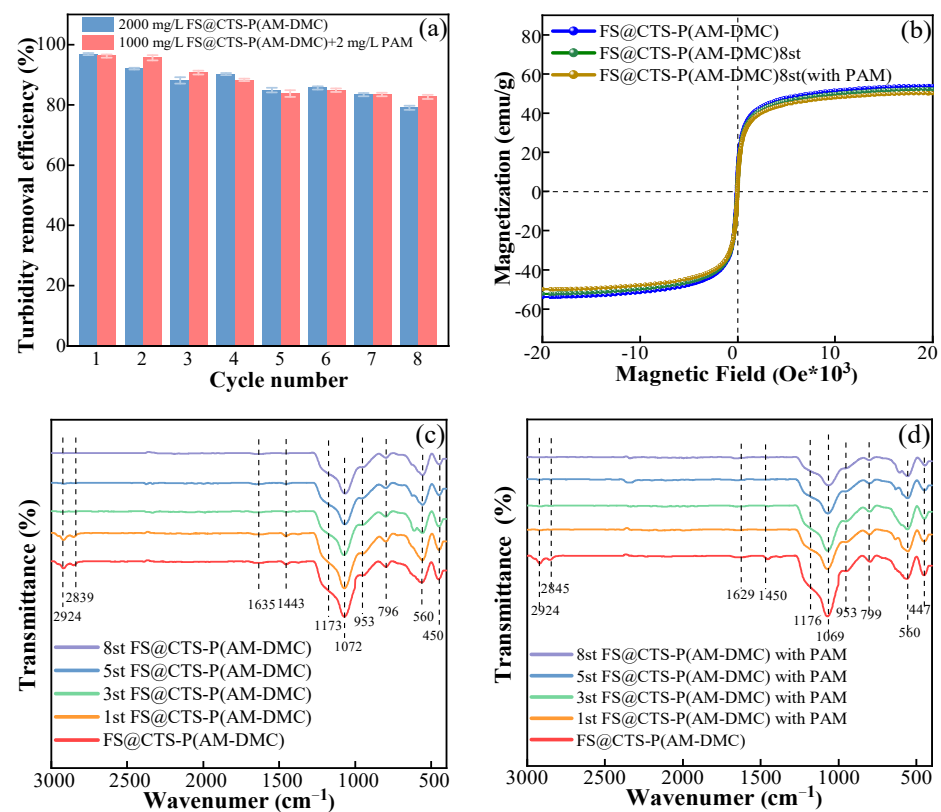
Figure 3. (**a**) Reusability of FS@CTS-P(AM-DMC) over eight cycles. (**b**) Magnetic hysteresis loops and (**c**,**d**) FT-IR spectra of two dosing modes of original and recycled FS@CTS-P(AM-DMC). Dosing mode: 2000 mg/L FS@CTS-P(AM-DMC) and 1000 mg/L FS@CTS-P(AM-DMC) + 2 mg/L PAM. pH = 7.0. Stirring time = 10 min. Settling time = 3 min.

3.3. Magnetic Flocculation Mechanism

3.3.1. Floc Size Distribution

The characteristics of flocs provide crucial insights into the flocculation process, which are essential for comprehending the flocculation mechanism [68,69]. First, the variations in the size distribution during rapid stirring and magnetic separation were investigated. At a pH value of 7.0, the floc size greatly increased from 9.29 μm to 63.1 μm during rapid stirring, followed by a gradual rise to 65.5 μm and subsequent stability (Figure 4a). As for the dosing mode involving PAM, the floc size steadily grew with the duration of rapid stirring, rising from 32.4 to 123 μm (Figure 4b). The rapid stirring converted the mechanical energy into fluid kinetic energy, thereby overcoming the energy barriers that hindered particle movement [70]. This energy conversion enhanced the frequency of collisions and interaction efficiency between the FS@CTS-P(AM-DMC) and emulsified oil droplets, further enlarging the floc particle size [71]. Moreover, unlike FS@CTS-P(AM-DMC) alone, the incorporation of PAM resulted in continuous floc growth and aggregation, promoting the formation of larger magnetic flocs. The large flocs facilitated their separation, thereby enhancing treatment effectiveness. Subsequently, during the magnetic separation stage, the floc particle size further increased, reaching 72.9 and 147 μm for the respective modes. This indicated that the magnetic flocs undergo further collisions and aggregation during magnetic separation, leading to the formation of even larger flocs.
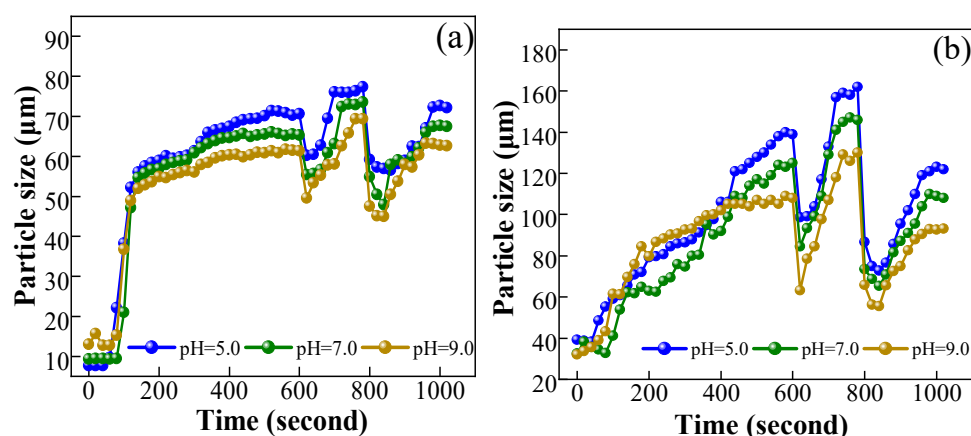
Figure 4. The evolution of floc size under (**a**) 2000 mg/L FS@CTS-P(AM-DMC) and (**b**) 1000 mg/L FS@CTS-P(AM-DMC) + 2 mg/L PAM. Stirring speed = 400 rpm. Stirring time = 10 min. Settling time = 3 min. Breakage time = 1 min. Regeneration time = 3 min.

To further understand the strength and regeneration capability of the flocs, fragmentation and regeneration tests were conducted. During the breakage stage at pH 7.0, shear forces disrupted the floc structure, reducing the floc size from 72.9 to 50.5 μm when using 2000 mg/L FS@CTS-P(AM-DMC) alone (Figure 4a). Despite this, the floc exhibited a high strength factor of 69.3%, apparently surpassing the 10–34% observed with conventional coagulants [72–74]. The magnetic flocs possessed a robust resistance to breakage, suggesting the ability of the magnetic force to produce dense magnetic flocs. In contrast, when PAM was added, although the floc size reached 68.7 μm, the strength factor sharply decreased to 46.7%. The magnetic flocs involving PAM were more susceptible to breakage. During the regeneration stage, the broken flocs recombined, forming rearranged flocs of 67.7 and 109 μm under the two dosing modes, respectively. The regeneration factor for FS@CTS-P(AM-DMC) alone was 76.8%, higher than the 51.5% observed with PAM assistance. The tight chain structure, disrupted by the hydrolysis of PAM, proved challenging to reform after breakage [75]. Additionally, the flocs formed primarily through net catching and sweeping tended to exhibit a lower regeneration capacity.

To assess the influence of the pH on floc growth, the variations in floc sizes were compared under various pH conditions. During rapid stirring, the magnetic flocs obtained were 70.3, 65.6, and 61.5 μm at pH 5.0, 7.0, and 9.0, respectively (Figure 4a). Similarly, for the PAM-added dosing mode, the floc size followed a comparable trend, reaching 140, 123, and 109 μm at the corresponding pH values (Figure 4b). Alkaline conditions were detrimental to the aggregation process between the magnetic material and emulsified oil droplets. The zeta potentials presented that both the surface charge of the emulsified oil droplets and FS@CTS-P(AM-DMC) decreased as the pH values increased (Figure 1d). Therefore, the electrostatic repulsion was stronger at pH 9.0, resulting in smaller floc sizes. The growth rates were observed to be 12.3 and 11.9 μm/min at pH 5.0 and 7.0, respectively, whereas at pH 9.0, it decreased to 9.78 μm/min (Table S7). After adding PAM, the corresponding growth rates accelerated, reaching 15.63, 14.86, and 14.32 μm/min, respectively. This indicated that the pH conditions not only affected the size of the formed flocs but also influenced the growth rate of the flocs.

3.3.2. Fractal Dimension of Magnetic Flocs

The fractal dimension (D_f) is a mathematical parameter used to quantify the complexity and morphological characteristics of the objects. It is defined by measuring the scaling relationship between the spatial occupancy and the geometric shape of the structure [76]. D_f is often employed to evaluate the compactness of flocs. High D_f values indicate a compact internal structure, whereas lower values suggest a loose structure [77]. As shown in Figure 5a, when using 2000 mg/L FS@CTS-P(AM-DMC) alone, the D_f values were 1.56,

1.51, and 1.48 at pH 5.0, 7.0, and 9.0, respectively. The flocs formed under acidic conditions were relatively denser. Due to the electrostatic neutralization effect, the combination of emulsified oil droplets and FS@CTS-P(AM-DMC) became tighter. In contrast, under alkaline conditions, the flocs exhibited a looser structure. This might be attributed to the gradual increase in electrostatic repulsion between them. When PAM was added, there was a general increase in the overall D_f values, reaching 1.68, 1.66, and 1.61 at pH 5.0, 7.0, and 9.0, respectively (Figure 5c). The addition of PAM resulted in denser and more compact flocs. In summary, under the combined effects of electrostatic attraction, adsorption bridging, and magnetic forces, emulsified oil droplets and FS@CTS-P(AM-DMC) formed the dense three-dimensional network floc, facilitating effective oil–water separation.
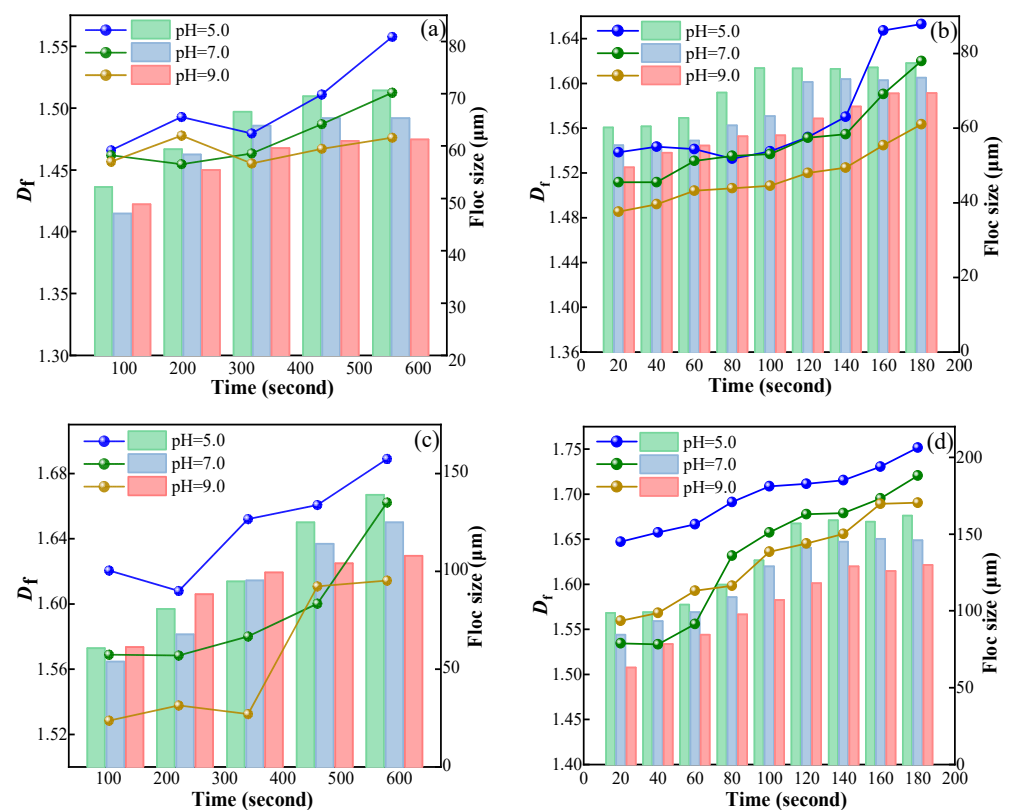
Figure 5. Variations in floc size and D_f during rapid stirring (**a**) and magnetic separation (**b**) for 2000 mg/L FS@CTS-P(AM-DMC) and (**c,d**) for 1000 mg/L FS@CTS-P(AM-DMC) + 2 mg/L PAM. Stirring speed = 400 rpm. Stirring time = 10 min. Settling time = 3 min.

The morphology and structure of magnetic flocs during rapid stirring and magnetic separation processes were investigated using microscopy and D_f analysis. When the pH was set at 7.0 for FS@CTS-P(AM-DMC), the D_f gradually increased from 1.46 at 2 min to 1.51 at 8 min during the rapid stirring (Figure 5a). Under the influence of magnetic dipoles, the magnetic flocs initially formed chain-like structures at 2 min (Figure S4a). Then, the network of magnetic flocs was formed at 8 min through constant collisions and aggregation. Unlike the dosing mode of FS@CTS-P(AM-DMC), the addition of PAM led to the appearance of small block-like flocs at 2 min (Figure S4b), with D_f increasing from 1.57 at 2 min to 1.66 at 10 min (Figure 5c). Subsequently, these small blocks aggregated to form larger block-like flocs within 10 min. This indicated that the addition of PAM facilitated the formation of block flocs in a short period of time, thereby achieving more effective oil–water separation.

During the magnetic separation process, both dosing modes demonstrated an increase in D_f. For FS@CTS-P(AM-DMC), the D_f increased from 1.51 to 1.62, whereas with PAM addition, it rose from 1.53 to 1.72 (Figure 4b,d). Similar flocculation processes were observed

in both cases, involving floc aggregation, chain-like floc formation, and the subsequent development of a reticular floc network (Figure S5). These observations underscored the ability of FS@CTS-P(AM-DMC) to generate larger and more compact magnetic flocs under the influence of a magnetic force. Overall, FS@CTS-P(AM-DMC) could form compact magnetic flocs, and it demonstrated advantages in rapidly removing emulsified oil droplets under the action of the applied magnetic field.

3.3.3. PIV Analysis of Velocity Field

The PIV method was employed to observe the velocity and direction of fluid flow of the magnetic flocs in the magnetic field [78], thereby allowing for an understanding of the dynamic characteristics of the flow field. For the usage of 2000 mg/L FS@CTS-P(AM-DMC) alone, the flow velocity of magnetic flocs reached 0.15 m/s, and the magnetic separation time was approximately 100 s (Figure 6a). The dosing mode with PAM had a faster flow rate of 0.15 m/s and shortened the magnetic separation time to 70 s (Figure 6b). This was attributed to the larger magnetic flocs formed with the addition of PAM, facilitating their rapid aggregation and swift movement under magnetic forces.

As shown in Figure 6a, the flow velocity and its spatial distribution gradually increased within the range of 2–30 s. At 30 s, the acceleration region aligned parallel to the magnetic field gradient, situated near the central area of the magnet, and the high flow velocity region was large. Eddies became distinctly visible at 50 s. The intensity of the eddies amplified with the prolonged separation time, and the regions of high flow velocity became concentrated at the peripheries of the eddies, where the relative motion was most pronounced. Due to the presence of eddies, flocs could collide and merge with each other during movement, ultimately forming large and dense flocs. After 20 s of accelerated motion, the magnetostriction speed gradually diminished. By 100 s, the magnetic separation was completed, and the subsequent variation in the flow field was mainly due to the flow of the solution itself.

For the dosing mode with PAM, the magnetic flocs underwent three stages of acceleration, stabilization, and deceleration. Notably, eddies were observed at 10 s of separation time (Figure 6b). This observation suggested that the motion and size of magnetic flocs influenced the distribution and velocity of the flow field during the magnetic separation process. Overall, PIV provided a highly intuitive display of the flow field velocity, motion patterns, and trajectories of oil-containing flocs during the magnetophoretic process, which facilitated the selection of suitable conditions for the flocculation processes.

3.3.4. Interaction Energy Analysis

The van der Waals, electrostatic, and total interaction energies between the FS@CTS-P(AM-DMC) and emulsified oil droplets were first investigated using the DLVO models. In the DLVO theory, the total interaction energy (U_{DLVO}) comprises the combined van der Waals potential energy (U_{vdw}) and the electrostatic potential energy (U_{EL}) between the particles [79]. As depicted in Figure 7a, the U_{DLVO} between emulsified oil droplets was measured to be 3125.2 K_BT at pH 3.0. With the increase in pH levels, the U_{DLVO} reached 8185.8 K_BT at pH 11.0. This indicated that as the pH gradually increased, emulsified oil droplets became more stable under alkaline conditions. As depicted in Figure 7b, no energy barrier existed between the FS@CTS-P(AM-DMC) and emulsified oil droplets at pH 3.0 and 5.0, indicating that they were easy to aggregate. Moreover, the predicted lines for the U_{DLVO} and U_{EL} values between the FS@CTS-P(AM-DMC) and emulsified oil droplets closely overlapped at pH 3.0 and 5.0 (Figure S7a,b). This meant that under acidic conditions, electrostatic interactions dominated the flocculation of emulsified oil droplets. Compared to the interaction energy between emulsified oil droplets, the energy barriers between the FS@CTS-P(AM-DMC) and emulsified oil droplets decreased to 966.5, 1312.3, and 3274.1 K_BT at pH 7.0, 9.0, and 11.0, respectively (Figure 7b). This hinted that the presence of FS@CTS-P(AM-DMC) significantly promoted the aggregation of emulsified oil droplets, despite the existence of an energy barrier between them.
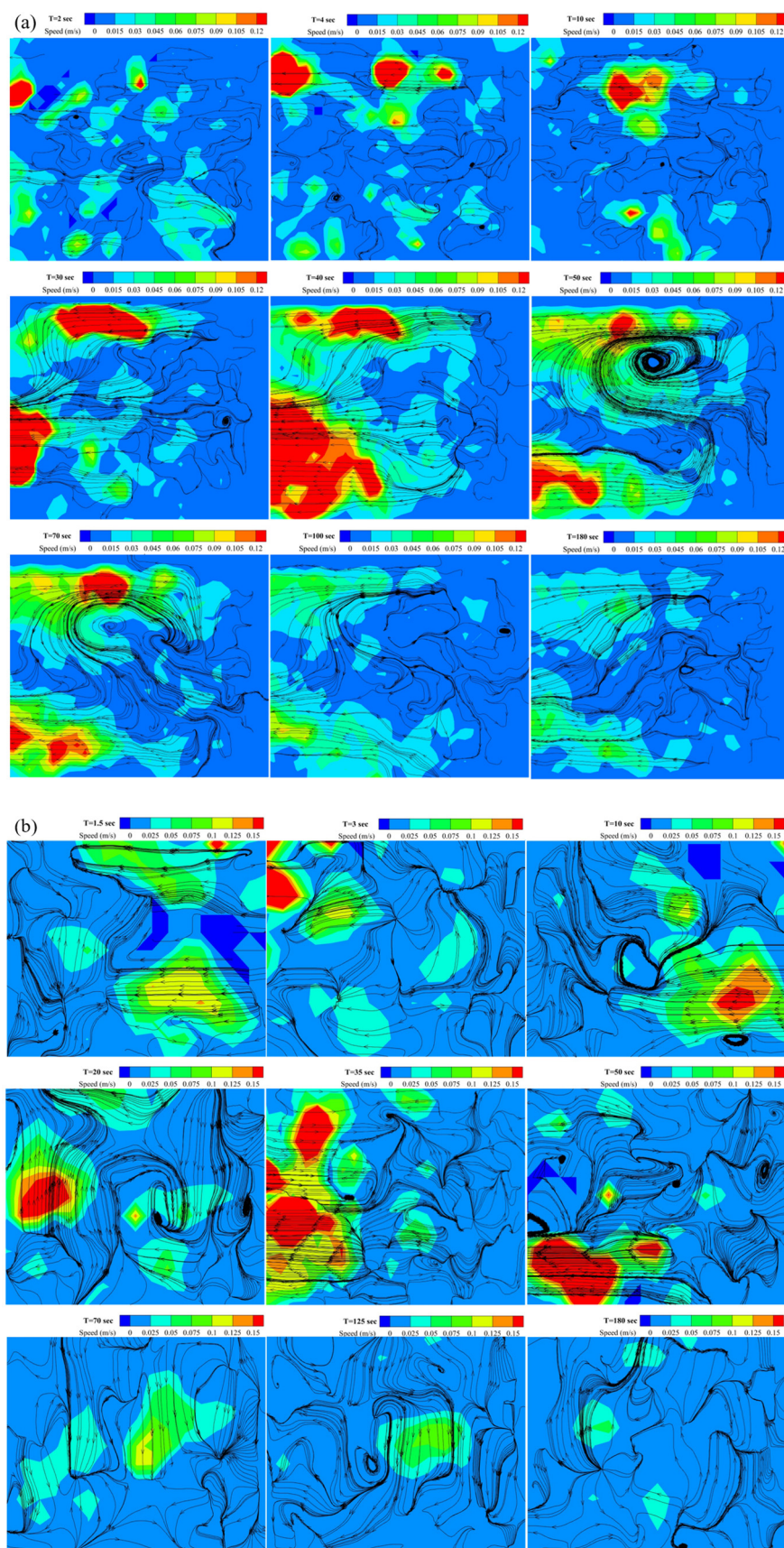
Figure 6. The magnetophoretic flow field under (**a**) 2000 mg/L FS@CTS-P(AM-DMC) and (**b**) 1000 mg/L FS@CTS-P(AM-DMC) + 2 mg/L PAM. pH = 7.0. Stirring speed = 400 rpm. Stirring time = 10 min. Settling time = 3 min.
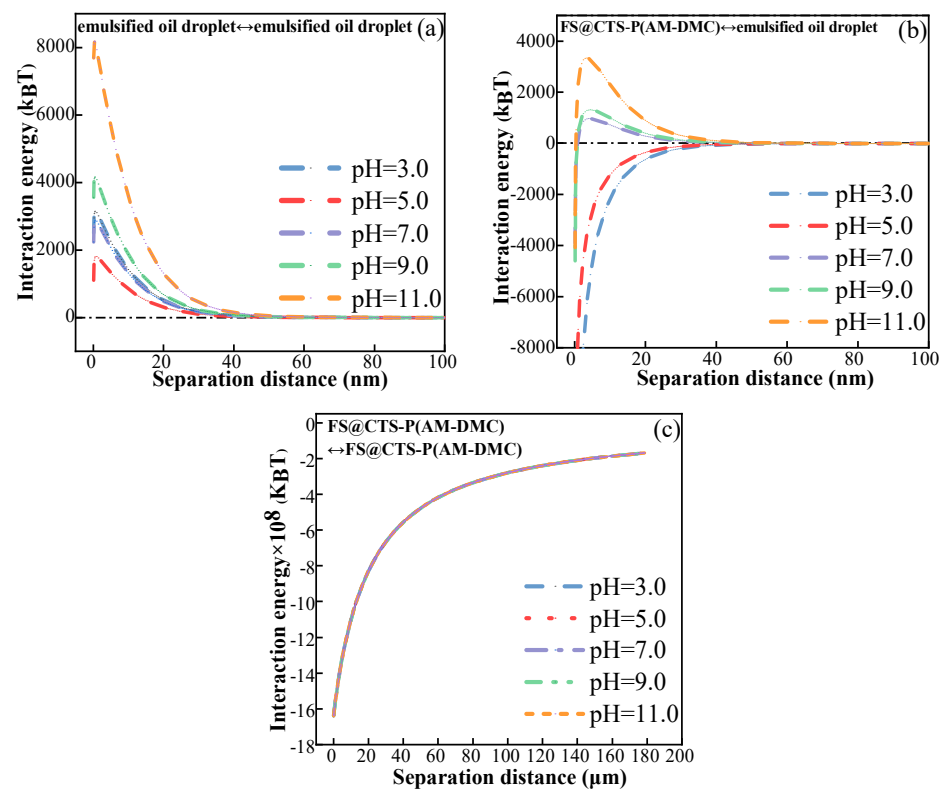
Figure 7. Interaction energy of DLVO between (**a**) oil emulsified droplet and oil emulsified droplet, (**b**) FS@CTS-P(AM-DMC) and oil emulsified droplet. Interaction energy of MDLVO between (**c**) FS@CTS-P(AM-DMC) and FS@CTS-P(AM-DMC).

In order to explore the hydration, hydrophilic, and hydrophobic interactions between the FS@CTS-P(AM-DMC) and emulsified oil droplets, calculations were performed using the EDLVO theoretical models [80]. The EDLVO models regard the interaction energy between particles as comprising van der Waals, electrostatic, and acid–base interaction energy [81]. The Lewis acid–base interaction energy (U_{AB}) represents the polarity interaction force between particles, encompassing the repulsion between particles caused by hydration effects as well as hydrophilic and hydrophobic effects [82]. In the present study, the ΔG_{AB} (h = h_0) values for emulsified oil droplet-to-emulsified oil droplet and FS@CTS-P(AM-DMC)-to-emulsified oil were determined to be -1.69×10^{-7} mJ m^{-2} and -2.09×10^{-7} mJ m^{-2}, respectively. The interaction energies calculated through the EDLVO models did not differ noticeably from those obtained through the DLVO models (Figure S9a,b). Hydrophobic interactions might occur when the water contact angle > 65°, leading to a reduction in the interaction energy and promoting particle aggregation [25,82,83]. The water contact angle of FS@CTS-P(AM-DMC) measured 13.1° (Table S4), indicating its hydrophilic nature. The presence of the emulsifier SDS conferred hydrophilic properties upon the emulsified oil droplets [84]. Therefore, there was no hydrophobic interaction between the FS@CTS-P(AM-DMC) and emulsified oil droplets.

Due to the introduction of an external magnetic field, magnetic forces become an important component among the interparticle forces alongside van der Waals, electrostatic, and acid–base interaction forces. Therefore, the magnetic interaction energy among the particles was further investigated using the MDLVO theory models. As illustrated in Figure 7c, the magnetic attraction between the FS@CTS-P(AM-DMC) was eight orders of magnitude higher than electrostatic and van der Waals forces, with no discernible energy barriers observed across a wide range of interaction distances (0–200 μm). This could be attributed to the high magnetic saturation (53.81 kA/m) and large particle size (radius = 10.3 μm) of FS@CTS-P(AM-DMC). Under various forces of interaction, such as van der Waals and

magnetic forces, FS@CTS-P(AM-DMC) and emulsified oil droplets formed chain-like and network-like magnetic flocs. And the magnetic flocs further collided and aggregated with each other under the influence of an external magnetic field, forming larger flocs. Notably, the magnetic forces could overcome the electrostatic repulsion between the negatively charged FS@CTS-P(AM-DMC) and emulsified oil droplets. This facilitated the collision and movement between them, achieving their effective removal at pH 7.0 and 9.0. However, at pH 11.0, the energy barrier between the emulsified oil droplets and FS@CTS-P(AM-DMC) was much higher, featuring strong electrostatic repulsion (3416.1 K_BT). Therefore, despite the high magnetic forces, the removal efficiency of emulsified oil droplets inevitably decreased under strongly alkaline conditions. This explained why flocculation could still be highly fulfilled at pH 7.0 and 9.0 without electro−neutralization, whereas at pH 11.0, its flocculation efficiency drastically declined.

4. Conclusions

In this study, FS@CTS-P(AM-DMC) demonstrated an outstanding efficacy in removing emulsified oil droplets in a wide pH range (3.0–9.0) and initial oil concentration range (200–3000 mg/L). Dosing 5000 mg/L FS@CTS-P(AM-DMC) alone achieved values of 98.7 and 88.9% for turbidity and COD removal, respectively, at pH 7.0 and an initial oil concentration of 3000 mg/L. Another dosing mode, namely FS@CTS-P(AM-DMC) with PAM, also demonstrated an effective flocculation efficiency. PAM addition could boost the particle size and D_f of the floc, therefore improving the removal efficiency and reducing the dose of FS@CTS-P(AM-DMC). However, the PAM-assisted mode was strongly influenced by the pH, with the flocculation efficiency dropping sharply at pH 11.0. And under varying magnetic field strengths, the removal efficiency was inferior compared to the use of FS@CTS−P(AM−DMC) alone. After eight cycles, the removal efficiency still remained above 79.0%, indicating the robust stability and reusability of FS@CTS-P(AM-DMC). Meanwhile, FS@CTS-P(AM-DMC) also demonstrated outstanding salt resistance, as K^+, Na^+, Ca^{2+}, and Mg^{2+} ions did not affect its flocculation performance. The floc size and D_f of magnetic flocs decreased with increasing pH values. However, the flocs exhibited high regeneration and resistance to fragmentation at pH 5.0, 7.0, and 9.0. Due to electrostatic attraction, van der Waals forces, and magnetic forces, FS@CTS-P(AM-DMC) and emulsified oil droplets colliding with each other formed chain and three-dimensional mesh magnetic flocs. During the magnetophoretic processes, eddies formed by the movement of magnetic flocs, facilitated the capture of residual emulsified oil droplets through sweeping and netting effects. The pH_{PZC} of FS@CTS-P(AM-DMC) was 6.6, and the zeta potential of emulsified oil droplets was negative in the range of pH 2.0–12.0. The electrical neutralization dominated under acidic conditions, while magnetic interactions were the main mechanism of magnetic flocculation under neutral and alkaline conditions. The remarkable performance of FS@CTS-P(AM-DMC) provided a new insight in the treatment of high-concentration emulsified, oily wastewater.

droplet and FS@CTS-P(AM-DMC) (a–e); Figure S8. Interaction energy versus interaction distance between different interacting entities: FS@CTS-P(AM-DMC) and FS@CTS-P(AM-DMC) (a–e); Figure S9. Interaction energy of EDLVO between (a) oil emulsified droplet and oil emulsified droplet, (b) FS@CTS-P(AM-DMC) and oil emulsified droplet; Table S1. Parameters used in DLVO, EDLVO and MDLVO equations [85]; Table S2. Characteristics of FS@CTS-P(AM-DMC) and emulsified oil droplet; Table S3. Surface tension and components of liquid (mJ/m^2) [86]; Table S4. The contact angles for flocculants and the calculated surface tension energy components; Table S5. The Hamaker constants for the interacting emulsified oil droplets and flocculants; Table S6. Comparison of the reported removal efficiency of different magnetic flocculants for emulsified oily wastewater [47,87–92]; Table S7. The properties of flocs under different dosing modes and pH levels.

Author Contributions: Conceptualization, methodology, software, investigation, and writing—original draft S.D.; formal analysis, visualization, and software, S.D. and C.L.; visualization and software, P.C.; writing—review and editing, supervision, and data curation, W.L. All authors have read and agreed to the published version of the manuscript.

Data Availability Statement: The data presented in this study are available on request from the corresponding author.

Conflicts of Interest: The authors declare no conflicts of interest.

References

1. Song, D.; Zheng, D.; Li, Z.; Wang, C.; Li, J.; Zhang, M. Research Advances in Wood Composites in Applications of Industrial Wastewater Purification and Solar-Driven Seawater Desalination. *Polymers* **2023**, *15*, 4712. [CrossRef] [PubMed]
2. Khan, M.J.; Wibowo, A.; Karim, Z.; Posoknistakul, P.; Matsagar, B.M.; Wu, K.C.-W.; Sakdaronnarong, C. Wastewater Treatment Using Membrane Bioreactor Technologies: Removal of Phenolic Contaminants from Oil and Coal Refineries and Pharmaceutical Industries. *Polymers* **2024**, *16*, 443. [CrossRef] [PubMed]
3. Xu, Y.; Wang, W.; Zhu, Z.; Xu, B. In Situ Fenton Triggered PDA Coating Copper Mesh with Underwater Superoleophobic Property for Oily Wastewater Pretreatment. *Processes* **2021**, *9*, 1665. [CrossRef]
4. Lü, T.; Qi, D.; Zhang, D.; Fu, K.; Li, Y.; Zhao, H. Fabrication of recyclable multi-responsive magnetic nanoparticles for emulsified oil-water separation. *J. Clean. Prod.* **2020**, *255*, 120293. [CrossRef]
5. He, J.; Zhao, H.; Li, X.; Su, D.; Zhang, F.; Ji, H.; Liu, R. Superelastic and superhydrophobic bacterial cellulose/silica aerogels with hierarchical cellular structure for oil absorption and recovery. *J. Hazard. Mater.* **2018**, *346*, 199–207. [CrossRef]
6. Medeiros, A.D.L.M.d.; Silva Junior, C.J.G.d.; Amorim, J.D.P.d.; Durval, I.J.B.; Costa, A.F.d.S.; Sarubbo, L.A. Oily Wastewater Treatment: Methods, Challenges, and Trends. *Processes* **2022**, *10*, 743. [CrossRef]
7. Azevedo, A.; Etchepare, R.; Calgaroto, S.; Rubio, J. Aqueous dispersions of nanobubbles: Generation, properties and features. *Miner. Eng.* **2016**, *94*, 29–37. [CrossRef]
8. Bastos, P.; Santos, M.; Carvalho, P.; Velizarov, S.; Crespo, J. Pilot scale reverse osmosis refinery wastewater treatment—A techno-economical and sustainability assessment. *Environ. Sci. Water Res. Technol.* **2021**, *7*, 549–561. [CrossRef]
9. Abdurahman, N.H.; Rosli, Y.M.; Azhari, N.H.; Hayder, G.; Norasyikin, I. A Hybrid Ultrasonic Membrane Anaerobic System (UMAS) Development for Palm Oil Mill Effluent (POME) Treatment. *Processes* **2023**, *11*, 2477. [CrossRef]
10. Wu, M.; Zhai, M.; Li, X. Adsorptive removal of oil drops from ASP flooding-produced water by polyether polysiloxane-grafted ZIF-8. *Powder Technol.* **2021**, *378*, 76–84. [CrossRef]
11. Ma, J.; Shi, J.; Ding, H.; Zhu, G.; Fu, K.; Fu, X. Synthesis of cationic polyacrylamide by low-pressure UV initiation for turbidity water flocculation. *Chem. Eng. J.* **2017**, *312*, 20–29. [CrossRef]
12. Jia, H.; Liu, W.; Wang, J.; Ngo, H.H.; Guo, W.; Zhang, H. Optimization of sensing performance in an integrated dual sensors system combining microbial fuel cells and upflow anaerobic sludge bed reactor. *Chemosphere* **2018**, *210*, 931–940. [CrossRef] [PubMed]
13. You, Z.; Zhang, L.; Zhang, S.; Sun, Y.; Shah, K. Treatment of Oil-Contaminated Water by Modified Polysilicate Aluminum Ferric Sulfate. *Processes* **2018**, *6*, 95. [CrossRef]
14. Parrino, F.; Corsino, S.F.; Bellardita, M.; Loddo, V.; Palmisano, L.; Torregrossa, M.; Viviani, G. Sequential biological and photocatalysis based treatments for shipboard slop purification: A pilot plant investigation. *Process Saf. Environ. Prot.* **2019**, *125*, 288–296. [CrossRef]
15. Liu, B.; Chen, X.; Zheng, H.; Wang, Y.; Sun, Y.; Zhao, C.; Zhang, S. Rapid and efficient removal of heavy metal and cationic dye by carboxylate-rich magnetic chitosan flocculants: Role of ionic groups. *Carbohydr. Polym.* **2018**, *181*, 327–336. [CrossRef]

16.   Du, C.; Hu, Y.; Han, H.; Sun, W.; Hou, P.; Liu, R.; Wang, L.; Yang, Y.; Liu, R.; Sun, L.; et al. Magnetic separation of phosphate contaminants from starch wastewater using magnetic seeding. *Sci. Total Env.* **2019**, *695*, 133723. [CrossRef]

17.   Zhang, L.; Verstraete, W.; de Lourdes Mendoza, M.; Lu, Z.; Liu, Y.; Huang, G.; Cai, L. Decrease of dissolved sulfide in sewage by powdered natural magnetite and hematite. *Sci. Total Env.* **2016**, *573*, 1070–1078. [CrossRef]

18.   Lü, T.; Chen, Y.; Qi, D.; Cao, Z.; Zhang, D.; Zhao, H. Treatment of emulsified oil wastewaters by using chitosan grafted magnetic nanoparticles. *J. Alloys Compd.* **2017**, *696*, 1205–1212. [CrossRef]

19.   Cai, D.; Zhang, T.; Zhang, F. Evaluation of oilfield-produced water treated with a prepared magnetic inorganic polymer: Poly(silicate aluminum)/magnetite. *J. Appl. Polym. Sci.* **2017**, *135*, 4. [CrossRef]

20.   Tang, J.; Wang, J.; Jia, H.; Wen, H.; Li, J.; Liu, W.; Li, J. The investigation on Fe_3O_4 magnetic flocculation for high efficiency treatment of oily micro-polluted water. *J. Env. Manag.* **2019**, *244*, 399–407. [CrossRef]

21.   Al-Rubaie, M.; Dixon, M.; Abbas, T. Use of flocculated magnetic separation technology to treat Iraqi oilfield co-produced water for injection purpose. *Desalination Water Treat.* **2013**, *53*, 2086–2091. [CrossRef]

22.   Ma, J.; Fu, X.; Jiang, L.; Zhu, G.; Shi, J. Magnetic flocculants synthesized by Fe_3O_4 coated with cationic polyacrylamide for high turbid water flocculation. *Env. Sci. Pollut. Res. Int.* **2018**, *25*, 25955–25966. [CrossRef] [PubMed]

23.   Bakhteeva, I.A.; Medvedeva, I.V.; Filinkova, M.S.; Byzov, I.V.; Zhakov, S.V.; Uimin, M.A.; Yermakov, A.E. Magnetic sedimentation of nonmagnetic TiO2 nanoparticles in water by heteroaggregation with Fe-based nanoparticles. *Sep. Purif. Technol.* **2019**, *218*, 156–163. [CrossRef]

24.   Liu, C.; Wang, X.; Qin, L.; Li, H.; Liang, W. Magnetic coagulation and flocculation of a kaolin suspension using Fe_3O_4 coated with SiO2. *J. Environ. Chem. Eng.* **2021**, *9*, 105980. [CrossRef]

25.   Wang, X.; Liu, C.; Qin, L.; Liang, W. Self-assembly of Fe_3O_4 with natural tannin as composites for microalgal harvesting. *Fuel* **2022**, *321*, 124038. [CrossRef]

26.   Zhou, J.; Sui, H.; Ma, J.; Xingang, L.; Al-Shiaani, N.; He, L. Fast demulsification of oil-water emulsions at room temperature by functionalized magnetic nanoparticles. *Sep. Purif. Technol.* **2021**, *274*, 118967. [CrossRef]

27.   Lü, T.; Qi, D.; Zhang, D.; Lin, S.; Mao, Y.; Zhao, H. Facile synthesis of N-(aminoethyl)-aminopropyl functionalized core-shell magnetic nanoparticles for emulsified oil-water separation. *J. Alloys Compd.* **2018**, *769*, 858–865. [CrossRef]

28.   Shao, S.; Li, Y.; Lü, T.; Qi, D.; Zhang, D.; Zhao, H. Removal of Emulsified Oil from Aqueous Environment by Using Polyvinylpyrrolidone-Coated Magnetic Nanoparticles. *Water* **2019**, *11*, 1993. [CrossRef]

29.   Ma, J.; Wu, G.; Zhang, R.; Xia, W.; Nie, Y.; Kong, Y.; Jia, B.; Li, S. Emulsified oil removal from steel rolling oily wastewater by using magnetic chitosan-based flocculants: Flocculation performance, mechanism, and the effect of hydrophobic monomer ratio. *Sep. Purif. Technol.* **2023**, *304*, 122329. [CrossRef]

30.   Ma, J.; Fu, X.; Xia, W.; Zhang, R.; Fu, K.; Wu, G.; Jia, B.; Li, S.; Li, J. Removal of emulsified oil from water by using recyclable chitosan based covalently bonded composite magnetic flocculant: Performance and mechanism. *J. Hazard. Mater.* **2021**, *419*, 126529. [CrossRef]

31.   Wang, R.; Cai, Y.; Su, Z.; Ma, X.; Wu, W. High positively charged Fe_3O_4 nanocomposites for efficient and recyclable demulsification of hexadecane-water micro-emulsion. *Chemosphere* **2022**, *291*, 133050. [CrossRef] [PubMed]

32.   Wang, H.; Zhang, X.; Fang, Y.; San, K.N.E.; Fan, Y. Smart and recyclable admicelle-coated Fe_3O_4 nanoparticles for treating oily wastewater. *J. Environ. Chem. Eng.* **2022**, *10*, 107445. [CrossRef]

33.   You, Z.; Xu, H.; Sun, Y.; Zhang, S.; Zhang, L. Effective treatment of emulsified oil wastewater by the coagulation-flotation process. *RSC Adv.* **2018**, *8*, 40639–40646. [CrossRef] [PubMed]

34.   Liu, C.; Wang, X.; Du, S.; Liang, W. Synthesis of chitosan-based grafting magnetic flocculants for flocculation of kaolin suspensions. *J. Environ. Sci.* **2024**, *139*, 193–205. [CrossRef] [PubMed]

35.   Liu, C.; Wang, X.; Du, S.; Cheng, P.; Liang, W. Magnetic coagulation and flocculation of kaolin suspension using Fe_3O_4 with plant polyphenol self-assembled flocculants. *Int. J. Biol. Macromol.* **2023**, *253*, 126578. [CrossRef] [PubMed]

36.   Xu, Z.; Zhu, Q.; Bian, J. Preparation of a recyclable demulsifier for the treatment of emulsified oil wastewater by chitosan modification and sodium oleate grafting Fe_3O_4. *J. Environ. Chem. Eng.* **2021**, *9*, 105663. [CrossRef]

37.   Hamedi, H.; Rezaei, N.; Zendehboudi, S. Investigation of Emulsified Oil Adsorption onto Functionalized Magnetic Nanoparticles— Kinetic and Isotherm Models. *Energies* **2023**, *16*, 8073. [CrossRef]

38.   Lu, J.-w.; Yuan, Z.-t.; Guo, X.-f.; Tong, Z.-y.; Li, L.-x. Magnetic separation of pentlandite from serpentine by selective magnetic coating. *Int. J. Miner. Metall. Mater.* **2019**, *26*, 1–10. [CrossRef]

39.   Tang, H.; Wang, L.; Sun, W.; Hu, Y.; Han, H.; Zhai, J. Electric arc furnace dust as magnetic carrier particles for removal of micro-fine particles from suspensions. *Sep. Purif. Technol.* **2017**, *176*, 220–230. [CrossRef]

40.   Paula, F.L.O.; Castro, L.L.; Cassiano, T.S.A.; dos Santos, S.G.; Gomide, G.; Depeyrot, J.; Campos, A.F.C. pH-dependent phase transitions in ferrofluids: A Monte Carlo simulation study using an extended DLVO model. *Colloids Surf. A Physicochem. Eng. Asp.* **2023**, *658*, 130578. [CrossRef]

41.   Shan, J.; Zhou, X. Starting Conditions of Particle Migration in Tight Sandstone Reservoir Development. *Processes* **2020**, *8*, 1491. [CrossRef]

42.   Zhang, C.; Dostál, J.; Heidinger, S.; Günther, S.; Odenbach, S. Experimental Investigation of a Pulsation Reactor via Optical Methods. *Processes* **2024**, *12*, 385. [CrossRef]

43. Fleischhauer, E.; Azimi, F.; Tkacik, P.; Keanini, R.; Mullany, B. Application of particle image velocimetry (PIV) to vibrational finishing. *J. Mater. Process. Technol.* **2016**, *229*, 322–328. [CrossRef]

44. Patalano, A.; García, C.M.; Rodríguez, A. Rectification of Image Velocity Results (RIVeR): A simple and user-friendly toolbox for large scale water surface Particle Image Velocimetry (PIV) and Particle Tracking Velocimetry (PTV). *Comput. Geosci.* **2017**, *109*, 323–330. [CrossRef]

45. Chen, H.; Qiu, Y.; Wang, H.; Gao, M. The Influence of a Manifold Structure on the Measurement Results of a PIV Flowmeter. *Processes* **2024**, *12*, 144. [CrossRef]

46. Sarno, L.; Tai, Y.-C.; Carravetta, A.; Martino, R.; Nicolina Papa, M.; Kuo, C.-Y. Challenges and improvements in applying a particle image velocimetry (PIV) approach to granular flows. *J. Phys. Conf. Ser.* **2019**, *1249*, 012011. [CrossRef]

47. Liang, J.; Du, N.; Song, S.; Hou, W. Magnetic demulsification of diluted crude oil-in-water nanoemulsions using oleic acid-coated magnetite nanoparticles. *Colloids Surf. A Physicochem. Eng. Asp.* **2015**, *466*, 197–202. [CrossRef]

48. Harford, A.J.; Hogan, A.C.; Jones, D.R.; van Dam, R.A. Ecotoxicological assessment of a polyelectrolyte flocculant. *Water Res.* **2011**, *45*, 6393–6402. [CrossRef] [PubMed]

49. Zhang, C.; Zhou, C.-l.; Zhou, Y.-c.; Shen, Y.; Wang, Y.-w.; Ge, S.-f. Study on the Effect of Coagulant Ratio on Dehydration Performance of Acrylic Sludge. *IOP Conf. Ser. Earth Environ. Sci.* **2018**, *146*, 012076. [CrossRef]

50. Nthunya, L.N.; Gutierrez, L.; Derese, S.; Mamba, B.B.; Verliefde, A.R.; Mhlanga, S.D. Adsorption of phenolic compounds by polyacrylonitrile nanofibre membranes: A pretreatment for the removal of hydrophobic bearing compounds from water. *J. Environ. Chem. Eng.* **2019**, *7*, 103254. [CrossRef]

51. Wu, L.J.; Gao, Y.; Xu, X.; Deng, J.; Liu, H. Excellent coagulation performance of polysilicate aluminum ferric for treating oily wastewater from Daqing gasfield: Responses to polymer properties and coagulation mechanism. *J. Environ. Manag.* **2024**, *356*, 120642. [CrossRef] [PubMed]

52. Kudryavtsev, Y.V.; Litmanovich, A.D.; Platé, N.A. On the Kinetics of Polyacrylamide Alkaline Hydrolysis. *Macromolecules* **1998**, *31*, 4642–4644. [CrossRef]

53. Nie, C.; Han, G.; Ni, J.; Guan, S.; Du, H.; Zhang, Y.; Wang, H. Stability Dynamic Characteristic of Oil-in-Water Emulsion from Alkali-Surfactant-Polymer Flooding. *ACS Omega* **2021**, *6*, 19058–19066. [CrossRef] [PubMed]

54. Sun, Z.; Li, Y.; Ming, X.; Chen, B.; Li, Z. Enhancing anti-washout behavior of cement paste by polyacrylamide gelation: From floc properties to mechanism. *Cem. Concr. Compos.* **2023**, *136*, 104887. [CrossRef]

55. Tang, C.C.; Zhang, X.Y.; Wang, R.; Wang, T.Y.; He, Z.W.; Wang, X.C. Calcium ions-effect on performance, growth and extracellular nature of microalgal-bacterial symbiosis system treating wastewater. *Env. Res.* **2022**, *207*, 112228. [CrossRef] [PubMed]

56. Ren, X.; Guo, L.; Chen, Y.; She, Z.; Gao, M.; Zhao, Y.; Shao, M. Effect of Magnet Powder (Fe$_3$O$_4$) on Aerobic Granular Sludge (AGS) Formation and Microbial Community Structure Characteristics. *ACS Sustain. Chem. Eng.* **2018**, *6*, 9707–9715. [CrossRef]

57. Hezave, A.Z.; Dorostkar, S.; Ayatollahi, S.; Nabipour, M.; Hemmateenejad, B. Investigating the effect of ionic liquid (1-dodecyl-3-methylimidazolium chloride ([C12mim] [Cl])) on the water/oil interfacial tension as a novel surfactant. *Colloids Surf. A Physicochem. Eng. Asp.* **2013**, *421*, 63–71. [CrossRef]

58. Pu, L.; Zeng, Y.J.; Xu, P.; Li, F.Z.; Zong, M.H.; Yang, J.G.; Lou, W.Y. Using a novel polysaccharide BM2 produced by Bacillus megaterium strain PL8 as an efficient bioflocculant for wastewater treatment. *Int. J. Biol. Macromol.* **2020**, *162*, 374–384. [CrossRef]

59. Liu, B.; Lu, H.; Wu, S.; Wang, Z.; Feng, L.; Zheng, H. Octopus tentacle-like molecular chains in magnetic flocculant enhances the removal of Cu(II) and malachite green in water. *Sep. Purif. Technol.* **2022**, *282*, 120139. [CrossRef]

60. Nwodo, U.; Agunbiade, M.; Green, E.; Mabinya, L.; Okoh, A. A Freshwater Streptomyces, Isolated from Tyume River, Produces a Predominantly Extracellular Glycoprotein Bioflocculant. *Int. J. Mol. Sci.* **2012**, *13*, 8679–8695. [CrossRef]

61. Lakshmanan, R.; Kuttuva Rajarao, G. Effective water content reduction in sewage wastewater sludge using magnetic nanoparticles. *Bioresour. Technol.* **2014**, *153*, 333–339. [CrossRef] [PubMed]

62. Park, J.A.; Kim, S.B. DLVO and XDLVO calculations for bacteriophage MS2 adhesion to iron oxide particles. *J. Contam. Hydrol.* **2015**, *181*, 131–140. [CrossRef] [PubMed]

63. Wang, J.; Liu, W.; Jia, H.; Zhang, H. Effects of recycling flocculation membrane filtration on drinking water treatment. *Aqua* **2013**, *62*, 433. [CrossRef]

64. Xu, B.; Zheng, C.; Zheng, H.; Wang, Y.; Zhao, C.; Zhao, C.; Zhang, S. Polymer-grafted magnetic microspheres for enhanced removal of methylene blue from aqueous solutions. *RSC Adv.* **2017**, *7*, 47029–47037. [CrossRef]

65. Hadizade, G.; Binaeian, E.; Emami, M.R.S. Preparation and characterization of hexagonal mesoporous silica/polyacrylamide nanocomposite capsule (PAM-HMS) for dye removal from aqueous solutioxns. *J. Mol. Liq.* **2017**, *238*, 499–507. [CrossRef]

66. Liu, Z.; Wei, H.; Li, A.; Yang, H. Evaluation of structural effects on the flocculation performance of a co-graft starch-based flocculant. *Water Res.* **2017**, *118*, 160–166. [CrossRef] [PubMed]

67. Shi, C.; Sun, W.; Sun, Y.; Chen, L.; Xu, Y.; Tang, M. Synthesis, Characterization, and Sludge Dewaterability Evaluation of the Chitosan-Based Flocculant CCPAD. *Polymers* **2019**, *11*, 95. [CrossRef] [PubMed]

68. Li, H.; Cai, T.; Yuan, b.; Li, R.; Yang, H.; Li, A. Flocculation of Both Kaolin and Hematite Suspensions Using the Starch-Based Flocculants and Their Floc Properties. *Ind. Eng. Chem. Res.* **2015**, *54*, 59–67. [CrossRef]

69. Machado, C.A.; Esteves, A.F.; Pires, J.C.M. Optimization of Microalgal Harvesting with Inorganic and Organic Flocculants Using Factorial Design of Experiments. *Processes* **2022**, *10*, 1124. [CrossRef]

70. Wu, Z.; Zeng, G.; Huang, J.; Xu, H.; Feng, J.; Song, P.; Li, M.; Wang, L. Assessing the effect of flow fields on flocculation of kaolin suspension using microbial flocculant GA1. *RSC Adv.* **2014**, *4*, 40464–40473. [CrossRef]
71. Wang, D.; Liu, Q. Hydrodynamics of froth flotation and its effects on fine and ultrafine mineral particle flotation: A literature review. *Miner. Eng.* **2021**, *173*, 107220. [CrossRef]
72. Yan, M.; Guo, K.; Gao, Y.; Yue, Q.; Gao, B. Insights into the control mechanism of different coagulation pretreatment on ultrafiltration membrane fouling for oily wastewater treatment. *Sep. Purif. Technol.* **2023**, *327*, 124907. [CrossRef]
73. Geng, Y.; Nie, Y.; Du, H.; Ma, T.; Li, L.; Zhao, C.; Xue, N.; Shen, Q. Coagulation performance and floc characteristics of Fe–Ti–V ternary inorganic coagulant for organic wastewater treatment. *J. Water Process Eng.* **2023**, *56*, 104344. [CrossRef]
74. Xu, W.; Gao, B. Effect of shear conditions on floc properties and membrane fouling in coagulation/ultrafiltration hybrid process—The significance of Alb species. *J. Membr. Sci.* **2012**, *415–416*, 153–160. [CrossRef]
75. Lipus, L.C.; Krope, J.; Crepinsek, L. Dispersion Destabilization in Magnetic Water Treatment. *J. Colloid. Interface Sci.* **2001**, *236*, 60–66. [CrossRef]
76. de Oliveira Anício, S.; dos Santos Lopes, V.; de Oliveira, A.L. PSD and Fractal Dimension for flocculation with different parameters and ferric chloride, aluminium polychloride and aluminium sulfate as coagulants. *J. Water Process Eng.* **2021**, *43*, 102180. [CrossRef]
77. Chen, Q.; Wang, Y. Influence of single- and dual-flocculant conditioning on the geometric morphology and internal structure of activated sludge. *Powder Technol.* **2015**, *270*, 1–9. [CrossRef]
78. Ban, Y.; Liu, L.; Du, J.; Ma, C. Investigation of the treatment efficiency and mechanism of microporous flocculation magnetic fluidized bed (MFMFB) reactor for Pb(II)-containing wastewater. *Sep. Purif. Technol.* **2024**, *334*, 125963. [CrossRef]
79. Salim, S.; Shi, Z.; Vermue, M.H.; Wijffels, R.H. Effect of growth phase on harvesting characteristics, autoflocculation and lipid content of Ettlia texensis for microalgal biodiesel production. *Bioresour. Technol.* **2013**, *138*, 214–221. [CrossRef]
80. Nabweteme, R.; Yoo, M.; Kwon, H.-S.; Kim, Y.J.; Hwang, G.; Lee, C.-H.; Ahn, I.-S. Application of the extended DLVO approach to mechanistically study the algal flocculation. *J. Ind. Eng. Chem.* **2015**, *30*, 289–294. [CrossRef]
81. Li, W.; Li, Y.; Xie, S.; Duan, W.; Chen, W. Roles and Influences of Kerosene on Chalcopyrite Flotation in MgCl2 Solution: EDLVO and DFT Approaches. *Minerals* **2022**, *12*, 48. [CrossRef]
82. Tanudjaja, H.J.; Chew, J.W. Assessment of oil fouling by oil-membrane interaction energy analysis. *J. Membr. Sci.* **2018**, *560*, 21–29. [CrossRef]
83. Chrysikopoulos, C.V.; Syngouna, V.I. Attachment of bacteriophages MS2 and PhiX174 onto kaolinite and montmorillonite: Extended-DLVO interactions. *Colloids Surf. B Biointerfaces* **2012**, *92*, 74–83. [CrossRef] [PubMed]
84. Song, S.; Zhang, H.; Sun, L.; Shi, J.; Cao, X.; Yuan, S. Molecular Dynamics Study on Aggregating Behavior of Asphaltene and Resin in Emulsified Heavy Oil Droplets with Sodium Dodecyl Sulfate. *Energy Fuels* **2018**, *32*, 12383–12393. [CrossRef]
85. Xu, J.; Yu, H.Q.; Li, X.Y. Probing the contribution of extracellular polymeric substance fractions to activated-sludge bioflocculation using particle image velocimetry in combination with extended DLVO analysis. *Chem. Eng. J.* **2016**, *303*, 627–635. [CrossRef]
86. Mohamed Noor, M.H.; Ngadi, N.; Mohammed Inuwa, I.; Opotu, L.A.; Mohd Nawawi, M.G. Synthesis and application of polyacrylamide grafted magnetic cellulose flocculant for palm oil wastewater treatment. *J. Environ. Chem. Eng.* **2020**, *8*, 104014. [CrossRef]
87. Hu, L.; Gao, S.; Ding, X.; Wang, D.; Jiang, J.; Jin, J.; Jiang, L. Photothermo-Responsive Single-Walled Carbon Nanotube-Based Ultrathin Membranes for On/Off Switchable Separation of Oil-in-Water Nanoemulsions. *ACS Nano* **2015**, *9*, 4835–4842. [CrossRef] [PubMed]
88. Duan, M.; Xu, Z.; Zhang, Y.; Fang, S.; Song, X.; Xiong, Y. Core-shell composite nanoparticles with magnetic and temperature dual stimuli-responsive properties for removing emulsified oil. *Adv. Powder Technol.* **2017**, *28*, 1291–1297. [CrossRef]
89. Mirshahghassemi, S.; Lead, J.R. Oil Recovery from Water under Environmentally Relevant Conditions Using Magnetic Nanoparticles. *Environ. Sci. Technol.* **2015**, *49*, 11729–11736. [CrossRef]
90. Xu, H.; Jia, W.; Ren, S.; Wang, J. Novel and recyclable demulsifier of expanded perlite grafted by magnetic nanoparticles for oil separation from emulsified oil wastewaters. *Chem. Eng. J.* **2018**, *337*, 10–18. [CrossRef]
91. Lu, T.; Zhang, S.; Qi, D.; Zhang, D.; Zhao, H. Enhanced demulsification from aqueous media by using magnetic chitosan-based flocculant. *J. Colloid Interface Sci.* **2018**, *518*, 76–83. [CrossRef] [PubMed]
92. Liang, J.; Li, H.; Yan, J.; Hou, W. Demulsification of Oleic-Acid-Coated Magnetite Nanoparticles for Cyclohexane-in-Water Nanoemulsions. *Energy Fuels* **2014**, *28*, 6172–6178. [CrossRef]